

CHAPTER VI

CORRECTING B_A COALESCENCE FACTOR

Our previous focuses have been on understanding the mechanisms and outcomes of cluster formation, particularly emphasizing the fireball geometry and the space-time picture. We found that the extracted (anti)nucleon source geometries, by fitting the experimental data on B_2 and $\overline{B_2}$ coalescence parameters, reveals a local maximum around $\sqrt{s_{NN}} = 27$ GeV. This source volume contradicts the conventional belief that the source volume grows with charged particle yields.

It is well-known and also mentioned before in Ch. V that the yield ratio of deuterons to nucleon square inversely scales with the volume $d/p^2 \propto 1/V$. In the thermal model, this volume corresponds to the volume of the thermal source, while the coalescence model suggests it corresponds to the spatial source where the clusters coalesce. Quantitatively, the relation between the density of nucleons N_p or N_n and the final cluster yield N_A based on the coalescence model is,

$$E_A \frac{d^3 N_A}{dp_A^3} = B_A \left(E_p \frac{d^3 N_p}{dp_p^3} \right)^Z \left(E_p \frac{d^3 N_n}{dp_n^3} \right)^N. \quad (6.1)$$

Here, $A = N + Z$ is the mass number of the produced nuclei. The coalescence parameter B_A is proportional to $(1/V)^{A-1}$. As mentioned above, the final values and the interpretation of the volume are model dependent (Butler and Pearson, 1963; Schwarzschild and Zupancic, 1963; Gutbrod et al., 1976; Bond et al., 1977; Sato and Yazaki, 1981; Gyulassy et al., 1983; Csernai and Kapusta, 1986; Mrowczynski, 1990). In the coalescence model, this volume is akin to the region of homogeneity interpreted by Hanbury-Brown-Twiss (HBT) analyses (Kapusta, 1980). This prompts further exploration to ascertain the compatibility between the coalescence volume and the HBT volume through the B_A values.

The comparison between experimental data of the coalescence factor B_A and predictions by HBT is illustrated in Figure 6.1. The HBT data (represented by the black dash-dotted line) aligns well with experimental data at high energies $E_{\text{beam}} > 10A$ GeV (Adamczyk et al., 2015). However, discrepancies emerge at lower

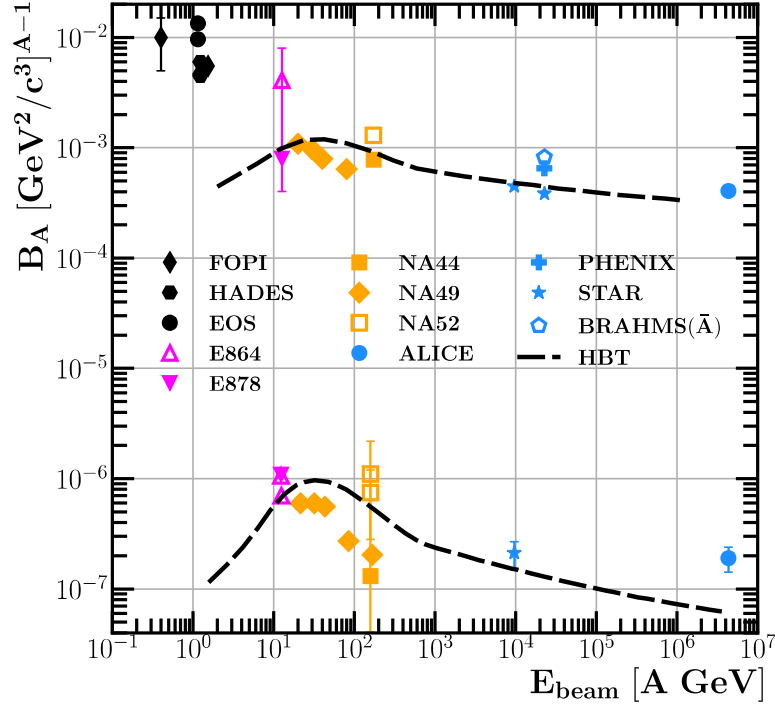


Figure 6.1 Coalescence parameter B_A measured by experiments (Braun-Munzinger and Dönigus, 2019) and predicted by HBT (Adamczyk et al., 2015) as a function of center-of-mass energy $\sqrt{s_{NN}}$ [GeV].

energies $E_{\text{beam}} \leq 10A$ GeV, raising questions as experimental measurements exhibit a notable spike in B_2 values, whereas the HBT prediction decreases.

In this chapter, our objective is to investigate and demonstrate that the observed discrepancy can be effectively addressed and resolved through a proper correction of the measured data. By implementing these corrections and testing with UrQMD simulations, we aim to not only solve the discrepancies at low collision energies but also enable the prediction of B_3 for the entire energy range under consideration.

6.1 Problems with B_A

We begin by addressing the issues with the measurements of B_2 as outlined in Eq. (6.1): First, the equation requires measurement of the neutron density, yet in practice, the estimated neutrons are obtained by assuming an equal number of neu-

trons and protons. Second, the measured protons typically represent the final-stage protons, which is justifiable only at high energies where cluster yields are significantly smaller than the square of final-stage protons.

At lower energies, however, the protons and neutrons in Eq. (6.1) are meant to be the primordial ones before coalescence, not the final-stage ones. At these energies, not only is there an enhancement in cluster production, but other clusters are also produced at mid-rapidity, drawing from the primordial protons and neutrons. This leads to a discrepancy of almost 40% compared to the final-stage nucleon contents, rendering the assumption of final-stage protons and neutrons unjustified. Additionally, the unequal distribution of protons to neutrons due to isospin equilibration further invalidates the assumption of equal nucleon distribution at low energies, as discussed in Ch. VII. Below we will investigate how to obtain the proper B_A for the experiments and present how do these effects affect the final results from the measurements.

6.2 Reconstructing Primordial Protons and Neutrons

6.2.1 Rapidity Distribution

We begin by illustrating the distinction between the final state protons typically measured by the experiments and the primordial protons before coalescence obtained from the simulations. To quantify these effects, we simulate the Au+Au 0 — 10% central collisions at $E_{\text{beam}} = 1.23A$ GeV using the UrQMD transport model, reflecting conditions attainable in current HADES experiments. As discussed above, at such low energy, the fraction of (light) clusters relative to the final state nucleons is substantial.

Figure 6.2 clearly illustrates the difference between the simulated primordial protons N_p^{prim} (red circles) and the final state protons N_p^{final} (red dashed line) in rapidity yields, with the final state protons accounting for only approximately 60% of the overall primordial protons before coalescence. This discrepancy arises because a portion of primordial protons is bound into light clusters. Based on this idea, we can estimate the primordial protons reconstructed from the measured final state protons by

$$\frac{dN_p^{\text{prim(reco)}}}{dy} = \frac{dN_p^{\text{final}}}{dy} + \sum_c^{\text{clusters}} Z_c \frac{dN_c^{\text{final}}}{dy}. \quad (6.2)$$

Here, the reconstructed primordial proton distribution $dN_p^{\text{prim(reco)}}/dy$ is estimated by

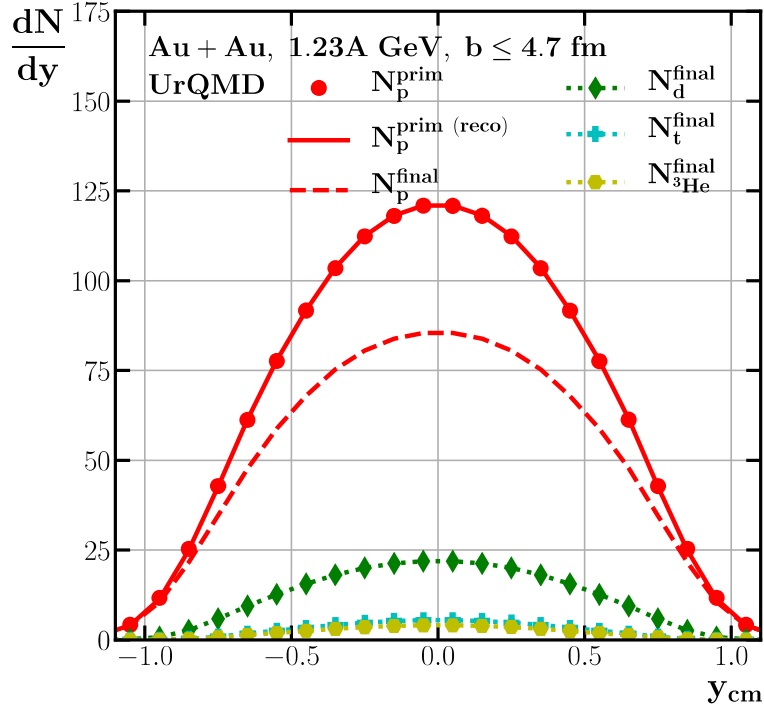


Figure 6.2 Rapidity distribution comparison of protons and light nuclei in 0 — 10% Au+Au collisions at $E_{\text{beam}} = 1.23A$ GeV. Simulated primordial protons (red circles), simulated final state protons (red dashed lines), and reconstructed primordial protons (red solid lines) are contrasted alongside the rapidity distributions of deuterons (green diamonds), tritons (cyan crosses), and ^3He nuclei (yellow hexagons).

adding all the final state proton contents, comprising the free final state protons dN_p^{final}/dy , along with the clusters dN_c^{final}/dy , where Z_c represents the proton number of the clusters c . The estimated reconstructed primordial proton distribution is depicted in Figure 6.2 as a red solid line, illustrating its high accuracy in describing the primordial proton distribution.

Similarly, a comparable approach as in Eq. (6.2) can be employed to estimate the primordial neutron numbers, given by

$$\frac{dN_n^{\text{prim(reco)}}}{dy} = \frac{dN_n^{\text{final}}}{dy} + \sum_c^{\text{clusters}} N_c \frac{dN_c^{\text{final}}}{dy}, \quad (6.3)$$

where N_c is the neutron number of cluster c . However, unlike protons, we lack experimental data on both the primordial and the final state neutron distributions. In order to estimate the final state neutrons, we consider the isospin configuration and the isospin exchange of the system. Initially the isospin contents are from two gold nuclei $2N_{Au}/2Z_{Au} = 1.49$. After the collision, isospin begins to exchange and equilibrate toward the final stage of the collision. The charged pions are emitted from the resonance decays carrying the isospin. The isospin exchange, transforming a primordial proton to a final stage neutron, produces a positively charged pion π^+ . On the other hand, the production of a negatively charged pion π^- represents the isospin exchange of a primordial neutron transformed into a final state proton. This implies that the integrated number of primordial protons and neutrons at given fixed participants A_{part} can be written as

$$N_p^{\text{prim(reco)}} = \frac{2Z_{Au}}{2A_{Au}}A_{part} + (N_{\pi^-} - N_{\pi^+}), \quad (6.4)$$

$$N_n^{\text{prim(reco)}} = \frac{2N_{Au}}{2A_{Au}}A_{part} - (N_{\pi^-} - N_{\pi^+}) \quad (6.5)$$

The first terms from both equations account for the isospin fraction from the gold nuclei to the participant numbers, i.e., estimated N_p^{part} and N_n^{part} . The second term subtracts and adds the primordial protons and neutrons from the final stage charged pions.

The participant numbers A_{part} cannot be measured directly. However, we can infer the number via $A_{part} = N_p^{\text{part}} + N_n^{\text{part}}$. Assuming the same isospin content ratio for the participants and the initial two gold nuclei which are well justify within the central collisions, we have $N_n^{\text{part}} \simeq \frac{2N_{Au}}{2Z_{Au}}N_p^{\text{part}}$. The number of participating protons can be calculated and measured via $N_p^{\text{part}} = N_p^{\text{prim}} - (N_{\pi^-} - N_{\pi^+})$. So, The participant numbers can be expressed in all measurable observables as

$$A_{part} = \left(N_p^{\text{prim}} - \Delta\pi \right) \times \left(\frac{2N_{Au}}{2Z_{Au}} \right), \quad (6.6)$$

*The UrQMD simulations give us the $\langle N_n^{\text{part}} \rangle = 2N_{Au} - \langle N_n^{\text{spec}} \rangle = 143.61$ and $\langle N_n^{\text{part}} \rangle = 2N_{Au} - \langle N_n^{\text{spec}} \rangle = 213.99$ which is $N_n^{\text{part}} \simeq \frac{2N_{Au}}{2Z_{Au}}N_p^{\text{part}} = 214.51$.

with $\Delta\pi \equiv (N_{\pi^-} - N_{\pi^+})$. Inserting this into Eq. (6.4) and Eq. (6.5), we finally obtain,

$$N_n^{\text{prim(reco)}} = N_p^{\text{prim(reco)}} \frac{\left(N_p^{\text{prim}} - \Delta\pi\right) \left(\frac{2N_{Au}}{2Z_{Au}} + 1\right) \frac{2N_{Au}}{2A_{Au}} - \Delta\pi}{\underbrace{\left(N_p^{\text{prim}} - \Delta\pi\right) \left(\frac{2N_{Au}}{2Z_{Au}} + 1\right) \frac{2N_{Au}}{2A_{Au}} + \Delta\pi}_{\equiv \Delta_{iso}^{\text{prim}}}}. \quad (6.7)$$

The factor $\Delta_{iso}^{\text{prim}}$ denotes the isospin ratio of the primordial state estimated from the integrated numbers in 4π . Now the reconstructed primordial neutron distribution Eq. (6.3) can now be expressed via the measured rapidity distributions of protons and clusters and the integrated number of charged pions $\Delta\pi$ in 4π . The primordial neutron rapidity distribution is then given by,

$$\frac{dN_n^{\text{prim(reco)}}}{dy} = \left(\frac{dN_p^{\text{final}}}{dy} + \sum_c^{\text{clusters}} Z_c \frac{dN_c^{\text{final}}}{dy} \right) \Delta_{iso}^{\text{prim}}. \quad (6.8)$$

Finally, the reconstructed final state neutron rapidity distribution reads

$$\frac{dN_n^{\text{final(reco)}}}{dy} = \left(\frac{dN_p^{\text{final}}}{dy} + \sum_c^{\text{clusters}} Z_c \frac{dN_c^{\text{final}}}{dy} \right) \Delta_{iso}^{\text{prim}} - \left(\sum_c^{\text{clusters}} N_c \frac{dN_c^{\text{final}}}{dy} \right). \quad (6.9)$$

The comparison of the UrQMD simulated neutron rapidity distributions with our reconstructions is depicted in Figure 6.3. We observe that the reconstructed neutron distributions from Eq. (6.8) (blue dashed line) and Eq. (6.9) (blue dotted line) match the results from simulations (blue squares), validating our proposed reconstruction method. Furthermore, we can observe that the neutron densities exceed the proton densities around $\simeq 1.3 - 1.5$ for both primordial and final states.

6.2.2 p_T Distribution

Proceeding from our successful testing of the reconstruction methods for estimating the differential rapidity distributions of primordial and final state neutrons and protons, we can now extend our analysis to the transverse momentum p_T distribution which is crucial for determining the coalescence parameter B_A . We follow the same procedure as for the rapidity distribution, but additionally scale the transverse momentum

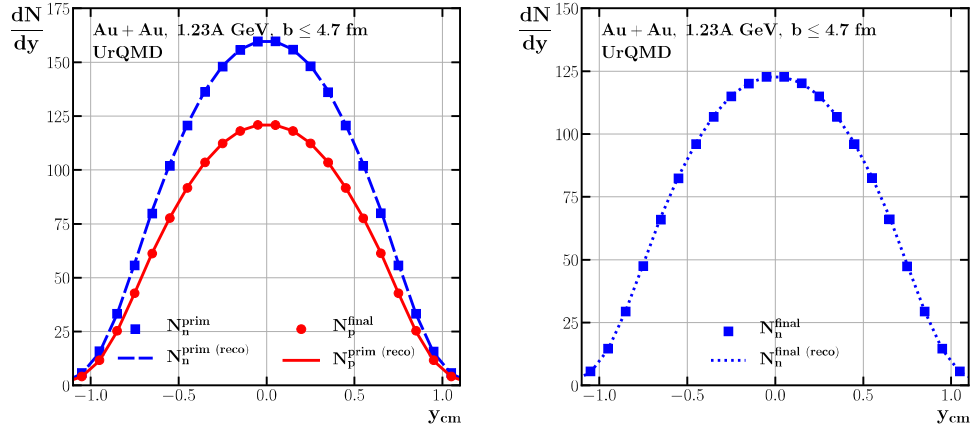


Figure 6.3 Rapidity distribution of simulated (symbols) and reconstructed (lines) proton and neutron at central Au+Au collisions $E_{\text{beam}} = 1.23A$ GeV. (Left panel) The comparison for the simulated and reconstructed primordial proton (red) and neutron (blue) rapidity based on Eq. (6.2) and Eq. (6.8). (Right panel) The comparison for the simulated and reconstructed final neutron rapidity based on Eq. (6.9).

of the clusters by their respective mass number, p_T/A . The reconstructed primordial proton and neutron transverse momentum distribution reads

$$\frac{1}{p_T} \frac{dN_p^{\text{prim(reco)}}}{dp_T} = \frac{1}{p_T} \frac{dN_p^{\text{final}}}{dp_T} + \sum_c^{\text{clusters}} Z_c \frac{1}{p_T/A} \frac{dN_c^{\text{final}}}{dp_T/A}, \quad (6.10)$$

$$\frac{1}{p_T} \frac{dN_n^{\text{prim(reco)}}}{dp_T} = \frac{1}{p_T} \frac{dN_n^{\text{final}}}{dp_T} + \sum_c^{\text{clusters}} N_c \frac{1}{p_T/A} \frac{dN_c^{\text{final}}}{dp_T/A}. \quad (6.11)$$

Figure 6.4 illustrates the invariant transverse momentum distributions of light clusters from our simulations, including deuterons (d: green diamonds), tritons (t: blue crosses), and ^3He (yellow hexagons), represented by dotted lines. Additionally, comparisons are made between simulated primordial neutrons (blue squares), protons (red circles), and the reconstructed primordial neutrons (dash-dotted lines) and protons (red solid line) at 0 — 10% central Au+Au collisions $E_{\text{beam}} = 1.23A$ GeV mid-rapidity, all at the same transverse momentum p_T/A . The calculations accurately depict both the reconstructed primordial protons and neutrons compared to their simulated counterparts. Additionally, the neutron density is higher than the proton density across the

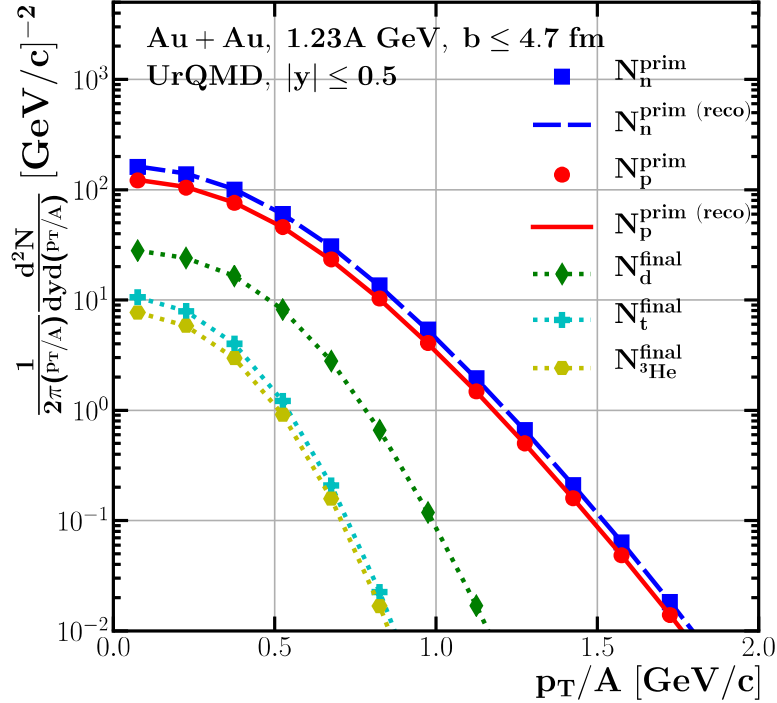


Figure 6.4 Invariant p_T spectra of d (green diamonds with dotted line), t (cyan pluses with dotted line), ^3He (yellow hexagons with dotted line), the primordial proton (full red circles) and neutron (full blue squares) from the simulations. While, the reconstructed primordial protons and neutrons are shown with solid red and solid blue lines respectively. The calculations are done at mid-rapidity in central Au+Au reactions at $E_{\text{beam}} = 1.23A$ GeV

entire transverse momentum range, consistent with the initial isospin asymmetry of the gold nuclei. This results in a higher abundance of tritons compared to ^3He nuclei in the coalescence spectra as expected.

We now discuss and clarify the use of the rapidity and p_T independence of $\Delta_{\text{ISO}}^{\text{prim}}$ from Eq. (6.7) for reconstructing primordial protons and neutrons with the 4π -integrated $\Delta\pi$. The pion rapidity and p_T distributions differ from those of participating nucleons. For instance, pion distributions are typically broader in rapidity due to their lower mass. Moreover, in p_T spectra, pions tend to have lower p_T values compared to nucleons. Consequently, applying a p_T -dependent correction would lead to increasingly severe corrections as p_T increases. Therefore, $\Delta_{\text{ISO}}^{\text{prim}}$ cannot be evaluated differ-

entially in rapidity and scaled transverse momentum p_T since it is also experimentally challenging to associate the rapidity and p_T bin of emitted pions with the corresponding primordial nucleons from their respective spectra. Figure 6.5 supports our approach and justifies the use of a constant $\Delta_{\text{iso}}^{\text{prim}}$ by demonstrating that $\Delta_{\text{iso}}^{\text{prim}}$ remains nearly constant across rapidity (left panel) and transverse momentum distributions p_T/A (right panel).

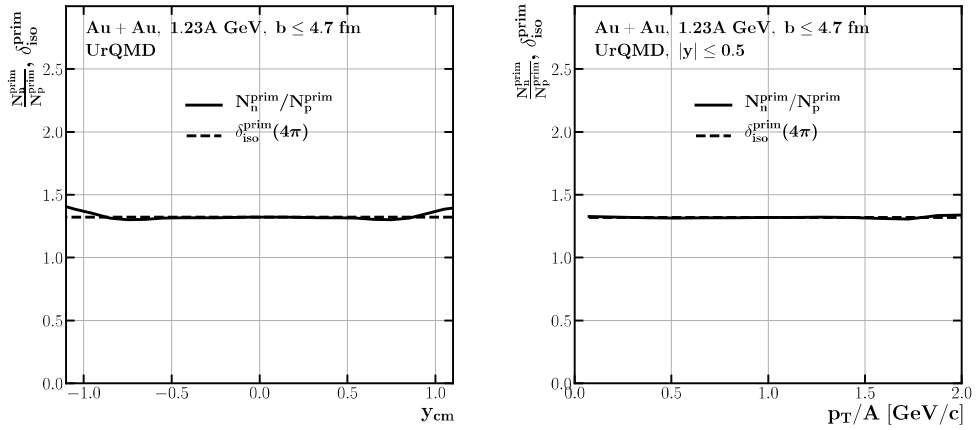


Figure 6.5 (Left panel) The Rapidity distributions of the neutron/proton ratio (full black line), and the integrated $\Delta_{\text{iso}}^{\text{prim}}$ (dashed line). (Right panel) The transverse momentum distributions of the primordial neutron/proton ratio (full black line), and the integrated $\Delta_{\text{iso}}^{\text{prim}}$ (dashed line). Both from UrQMD for 0 — 10% central Au+Au reactions at $E_{\text{beam}} = 1.23\text{A GeV}$

6.2.3 Estimating B_2 and B_3

We finally can test the impact of the invariant distribution of the (reconstructed) primordial protons and neutrons as a function of transverse momentum per nucleon p_T/A on the coalescence parameter B_A (Eq. (6.1)),

$$B_A = \left(\frac{1}{2\pi(p_T/A)} \frac{d^2 N_A}{dyd(p_T/A)} \right) / \left(\frac{1}{2\pi p_T} \frac{d^2 N_p}{dyd(p_T)} \right)^Z \cdot \left(\frac{1}{2\pi p_T} \frac{d^2 N_n}{dyd(p_T)} \right)^N. \quad (6.12)$$

Figure 6.6 illustrates the dependence of the coalescence parameters B_2 (left panel) and B_3 (right panel) on the scaled transverse momentum p_T/A .

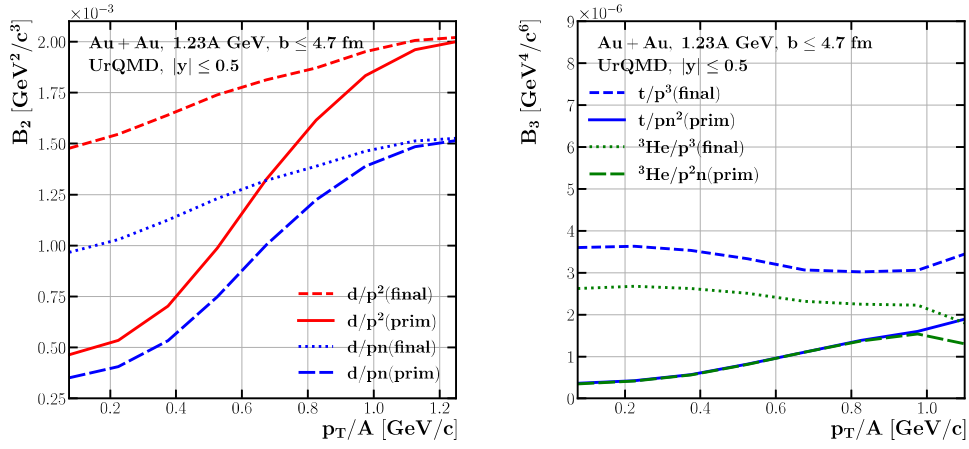


Figure 6.6 The scaled transverse momentum p_T/A -dependence of the coalescence parameter B_2 (left panel) and B_3 (right panel) calculated using the final state nucleons and reconstructed primordial nucleons from UrQMD for 0 — 10% central Au+Au reactions at $E_{\text{beam}} = 1.23A$ GeV

First, considering the impact of using final state neutrons for calculating the coalescence parameter, the original B_2 obtained by the final state proton squared ratio $d/p^2(\text{final})$ (red dashed line) already overestimates B_2 calculated with the product of final state protons and neutrons $d/pn(\text{final})$ (blue dotted line) by a factor ≈ 1.5 across the entire range of p_T/A . This p_T -independent scaling is attributed to the isospin asymmetry from the initial stage, aligning with the expected values from the initial isospin of gold nuclei $N_{\text{Au}}/Z_{\text{Au}} = 1.49$ and the primordial isospin factor $\Delta_{\text{iso}}^{\text{prim}} = 1.32$.

Second, upon changing from final state to primordial nucleons, B_2 calculated with the reconstructed primordial protons $d/p^2(\text{prim})$ (red solid line) noticeably suppresses the original $B_2 \propto d/p^2(\text{final})$ (red dashed line) across the entire p_T spectrum, with a maximum suppression factor of approximately 3 at $p_T/A \simeq 0$, gradually decreasing to unity for $p_T/A > 1.0$. This arises because clusters are more likely to coalesce at lower p_T/A than at higher p_T/A (see Figure 6.4), resulting in similar numbers of final and primordial protons and neutrons.

With the complete correction of the coalescence parameter calculated using the product of primordial protons and neutrons $d/pn(\text{prim})$ (blue dash-dotted line), it is evident that this correction further suppresses B_2 calculated using primordial proton square (red solid line) by a factor of 1.2 — 1.5, and around 4 times at p_T/A when compared to the original B_2 (red dashed line).

Similarly, in Figure 6.6 (right panel), the correction impacts on the original B_3 of tritons and ${}^3\text{He}$ calculated using the final state proton cubic square, i.e., t/p^3 (blue dashed line) and ${}^3\text{He}$ (green dotted line), are shown. The total corrections of B_3 tritons using primordial proton and neutrons squared (blue solid line) suppress their original B_3 (blue dashed line) by a factor of 7, while the corrected B_3 of ${}^3\text{He}$ using the primordial neutron and proton squared (green dash-dotted line) is suppressed by approximately 5 times its original B_3 value (green dotted line). Interestingly, the original values of B_3 for tritons (blue dashed line) and ${}^3\text{He}$ (green dotted line) are initially separated by an isospin factor of $1.2 - 1.5$. However, after the correction, both become identical for $p_T/A \leq 1.0$.

Finally, we arrive at our main objective of investigating the energy dependence of the coalescence parameter B_A and its comparison with experimental data (Wang et al., 1995; Ambrosini et al., 1998; Armstrong et al., 1999; Ahle et al., 1999; Barrette et al., 2000; Armstrong et al., 2000; Afanasiev et al., 2000; Bearden et al., 2002; Anticic et al., 2004; Anticic et al., 2016; Botvina et al., 2021). The representing coalescence parameter B_A is chosen at $p_T/A = 0$ [GeV/c] for each beam energy as we follow the HADES approach. Figure 6.7 shows our analyses of B_2 (left panel) and B_3 (right panel) from the original calculations and the corrected version comparing with the experimental data depicted by the symbols and the result from the HBT (Adamczyk et al., 2015) shown as a black dash-dotted line.

In the left panel, the original B_2 calculated by the final state proton square (red dashed line) increases after $E_{\text{beam}} \leq 10$ A GeV, consistent with FOPI and HADES experiments (black symbols). However, the corrected B_2 from our reconstructed primordial protons and neutrons (red solid line) aligns with the prediction from the HBT volume, decreasing with the energy for $E_{\text{beam}} \leq 10$ A GeV. The values of B_2 are summarized in Table 6.1

The same trend is evident in the calculation of B_3 in the right panel. The original B_3 values for both triton and ${}^3\text{He}$ (blue dashed line and green dotted line) obtained from the final state cubed proton number increase at lower beam energies, where the discrepancy in their isospin asymmetry by a factor of $1.2 - 1.5$ becomes more noticeable. This discrepancy arises because at lower energies, the system struggles to equilibrate the isospin due to time constraints and limited pion production for isospin exchange. In contrast, the corrected versions of B_3 for triton and ${}^3\text{He}$ exhibit almost identical behavior, decreasing with energy in qualitative agreement with the HBT predic-

Table 6.1 The B_2 values calculated final state protons and both primordial protons and neutrons at $p_T/A = 0.0$ GeV at midrapidity $|y| \leq 0.5$. The calculation is extracted from 0 — 10% central Au+Au collisions at kinetic beam energies from $E_{\text{beam}} = 0.3A$ to 40A GeV.

$E_{\text{beam}} [A \text{ GeV}]$	$B_2 [\times 10^{-4} \text{GeV}^2/c^3]$	
	d/p_{final}^2	$d/p_{\text{prim}} n_{\text{prim}}$
0.3	14.44	0.70
0.5	15.31	1.10
1.23	14.77	3.52
1.93	13.44	5.00
11.45	9.34	6.88
20	8.39	6.71
30	7.72	6.46
40	7.22	6.21

Table 6.2 The B_3 values calculated final state protons and both primordial protons and neutrons at $p_T/A = 0.0$ GeV at midrapidity $|y| \leq 0.5$. The calculation is extracted from 0 — 10% central Au+Au collisions at kinetic beam energies from $E_{\text{beam}} = 0.3A$ to 40A GeV.

$E_{\text{beam}} [A \text{ GeV}]$	$B_3^t [\times 10^{-7} \text{GeV}^4/c^6]$		$B_3^{\text{He}} [\times 10^{-7} \text{GeV}^4/c^6]$	
	t/p_{final}^3	$t/p_{\text{prim}} n_{\text{prim}}^2$	${}^3\text{He}/p_{\text{final}}^3$	${}^3\text{He}/p_{\text{prim}}^2 n_{\text{prim}}$
0.3	82.75	0.73	61.17	0.80
0.5	72.93	1.16	50.16	1.16
1.23	36.00	3.64	26.24	3.50
1.93	23.35	4.72	18.25	4.63
11.45	7.94	4.78	7.29	4.83
20	6.22	4.29	5.79	4.22
30	5.25	3.91	4.83	3.81
40	4.58	3.56	4.18	3.41

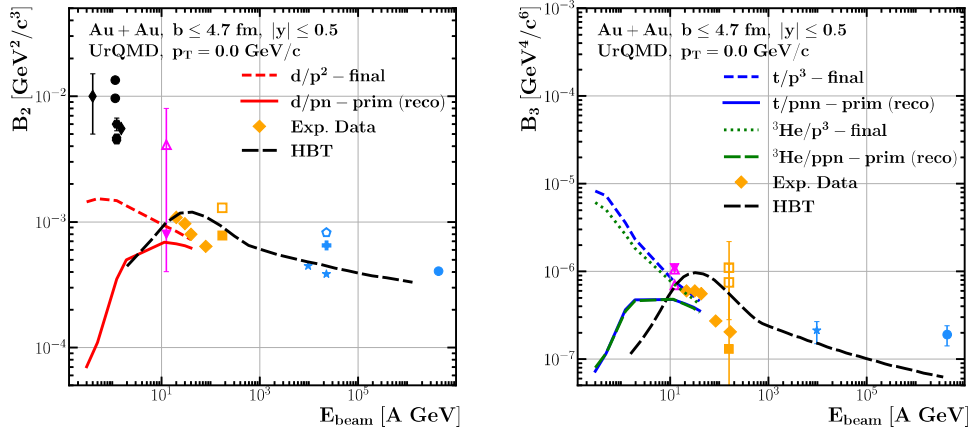


Figure 6.7 The figure caption describes the beam energy dependence of B_2 extracted at $p_T/A = 0$ GeV in mid-rapidity $|y| \leq 0.5$ for 0 – 10% central Au+Au collisions. Left panel: The dashed red line illustrates the original calculation of B_2 using the final state proton square, while the solid red line shows the corrected B_2 calculated by the product of reconstructed primordial protons and neutrons. Right panel: the original B_3 of tritons and ${}^3\text{He}$, calculated from the final state proton cubic square, are depicted by the blue dashed line and green dotted line while the corrected B_3 of tritons and ${}^3\text{He}$, using our reconstructed primordial protons and neutrons, are shown as the blue solid line and the green dash-dotted line, respectively. Experimental data (Wang et al., 1995; Ambrosini et al., 1998; Armstrong et al., 1999; Ahle et al., 1999; Barrette et al., 2000; Armstrong et al., 2000; Afanasiev et al., 2000; Bearden et al., 2002; Anticic et al., 2004; Anticic et al., 2016; Botvina et al., 2021) are denoted by symbols, while the dash-dotted black line represents the volume extracted from HBT results from STAR (Adamczyk et al., 2015).

tion. In this case, the splitting in isospin is already canceled out within each individual B_3 value, as mentioned above. The values of B_3 are summarized in Table 6.2.

In conclusion, we have investigated the discrepancy of the energy dependence of the coalescence parameters B_A between direct data from experiments and the prediction from HBT. Although the interpretation of $B_A \propto (1/V)^{A-1}$ is well-known and widely accepted, problems occur in its application. In the experiment, the measured B_A grows with decreasing energy. At first glance, this makes sense since the volume should also drop with energy if the cluster productions are not zero. However, the measurements of B_A not only estimate the number of neutrons from protons but

also use the final state protons in the calculations. However, we show that the coalescence parameter B_A , in fact, requires the primordial protons and neutrons as they are the main ingredients for the cluster before coalescence, i.e., the B_A is based on the probability with which the nucleons are drawn from the primordial state, not the final state. Thus, we obtain a method to acquire/reconstruct the primordial protons and neutrons from the final state observables and a corrected B_A . As expected, our calculation of the energy dependence of both B_2 and B_3 explains this discrepancy as supported by the HBT predictions.